ORIGINAL ARTICLE

Regional CBF changes in Parkinson's disease: a correlation with motor dysfunction

**Jung-Lung Hsu · Tzyy-Ping Jung · Chien-Yeh Hsu ·
Wei-Chih Hsu · Yen-Kung Chen · Jeng-Ren Duann ·
Han-Cheng Wang · Scott Makeig**

Abstract
Purpose The purpose of this study was to further localize cerebral perfusion abnormalities, and to better correlate these abnormalities with the clinical severity of Parkinson's disease (PD).
Methods A single-photon emission computed tomography (SPECT) study was performed on 27 patients with PD and 24 age-matched controls. SPECT images were spatially normalized, concatenated, and then decomposed using Infomax independent component analysis (ICA). The resulting image components were separated by logistic regression into two subspaces: "disease-related" components whose subject weights differed between groups, and

An editorial commentary on this paper is available at http://dx.doi.org/10.1007/s00259-007-0411-8

J.-L. Hsu · W.-C. Hsu · H.-C. Wang (✉)
Department of Neurology,
Shin Kong Wu Ho-Su Memorial Hospital,
95, Wen Chang Road, Shih Lin District,
Taipei, Taiwan
e-mail: drhan@ms1.hinet.net

J.-L. Hsu · C.-Y. Hsu
Graduate Institute of Medical Informatics,
Taipei Medical University,
Taipei, Taiwan

Y.-K. Chen
Department of Nuclear Medicine and PET Center,
Shin Kong Wu Ho-Su Memorial Hospital,
Taipei, Taiwan

J.-L. Hsu · T.-P. Jung · J.-R. Duann · S. Makeig
Computational Neurobiology Laboratory, The Salk Institute,
La Jolla, CA 92037-5800, USA

T.-P. Jung · J.-R. Duann · S. Makeig
Institute for Neural Computation, University of California,
San Diego, CA 92093, USA

"disease-unrelated" components. The resultant regional cerebral blood flow (rCBF) subspace images were normalized to global CBF for each subject, and then processed using statistical parametric mapping to compare rCBF values between PD and control subjects.
Results In the disease-related image subspace, patients with PD exhibited significantly higher adjusted rCBF in the putamen, globus pallidum, thalamus, brainstem, and the anterior lobe of the cerebellum, and significant hypoperfusion in the parieto-temporo-occipital cortex, the dorsolateral prefrontal cortex, the insula, and the cingulate gyrus. The motor Unified Parkinson's Disease Rating Scale scores correlated negatively with rCBF in the insula and cingulate gyrus. In the disease-unrelated image subspace, no brain voxels exhibited a significant group difference.
Conclusion ICA-based separation of normalized images into disease-related and disease-unrelated subspaces revealed many disease-related group blood flow differences. The regions revealed by ICA are consistent with the current model of PD. These rCBF changes in PD have not been fully demonstrated in any single functional imaging study previously.

Keywords SPECT · Parkinson's disease ·
Regional cerebral blood flow · Independent component
analysis · Statistical parametric mapping

Introduction

Parkinson's disease (PD) is a common neurodegenerative disease with four cardinal motor features: resting tremor, bradykinesia, cogwheel rigidity, and postural instability. The pathophysiological mechanisms of PD remain largely unknown, but the primary neurotransmitter deficit appears to be the loss of dopaminergic nigrostriatal neurons in

substantia nigra pars compacta [1], resulting in a loss of brain dopamine, most prominently in the striatum. According to the basal ganglia circuit model of PD [2, 3], the loss of dopaminergic innervation results in abnormal activities in the globus pallidus. These abnormal activities contribute directly and indirectly to the movement abnormalities observed in PD. Although the correlations between motor features and their cerebral substrates are not yet completely understood, a common expectation is that the alteration of functional activity in the basal ganglia in PD patients will be associated with changes in regional cerebral metabolism (rCMR) and regional cerebral blood flow (rCBF) in certain brain areas.

^{99m}Tc-HMPAO single-photon emission computed tomography (SPECT) is a well-established method of assessing rCBF. SPECT data have been analyzed utilizing either region of interest analysis [4], which investigates blood flow abnormalities in predefined regions, or statistical parametric mapping (SPM), which can generate images of blood flow abnormalities for each voxel in the whole brain image. Results of previous reports regarding rCBF differences between PD patients and controls have been mixed. In the basal ganglia, for example, rCBF has been reported to be reduced [5], increased [6, 7] or unchanged [8]. Recently, results reported by Imon et al. [9] showed that stage 1 or 2 PD patients had adjusted rCBF increases in bilateral putamen and the right hippocampus, while stage 3 or 4 patients had increases in bilateral putamen, globus pallidus, hippocampus, cerebellar hemispheres (dentate nuclei), left ventrolateral thalamus, right insula, and right inferior temporal gyrus.

As is now widely acknowledged, functional neuroimaging analytical methods utilizing model-driven approaches, such as SPM, are largely univariate and depend on some hypotheses on the data they are dealing with. There are complementary methods using data-driven approaches, such as principal component analysis, clustering analysis, and blind source separation, which are multivariate. These multivariate approaches have contributed greatly to studies on disease-related changes in patterns of functional connectivity [10, 11]. In a recent study, principal component analysis was utilized on [^{18}F]fluorodeoxyglucose positron emission tomography (FDG-PET) data combined with multivariate network analysis at a group level. The results from that approach can serve as an indicator of PD severity that is better than the univariate approaches [10].

Independent component analysis (ICA), also a multivariate approach, is a recently developed data-driven approach to imaging data analysis [12]. It has been widely applied to analyses of functional neuroimaging data, including electroencephalography, magnetoencephalography, event-related potential, functional magnetic resonance imaging (fMRI) [13], and other biomedical signals. ICA methods effectively

separate artifact components from fMRI data [14]. In the present study ICA was used to remove the disease-unrelated SPECT activity, including artifacts and rCBF unaffected by PD. Voxel-based SPM was then applied for analysis. It was hoped that this novel approach would reveal more areas of significant rCBF changes with better clinical correlation in PD patients.

Materials and methods

Subjects

Twenty-seven PD patients and 24 age-matched control subjects participated in the study. Patients were diagnosed with PD according to the research diagnostic criteria of Ward and Gibb [15]. Hoehn and Yahr method was used for disease staging [16]. The PD patients (21 male, 6 female; mean age 65.6±10 years) were divided into three groups: six at Hoehn and Yahr stage I, ten at stage II, and 11 at stage III. Patients' motor symptoms were clinically evaluated using the motor part of the Unified Parkinson's Disease Rating Scale (UPDRS) prior to the SPECT study [17]. The patients had been maintained on stable anti-parkinsonian therapy with optimal clinical benefit for at least 1 month before the study. Medications included various combinations of L-dopa with decarboxylase inhibitor (carbidopa), dopamine agonists, anticholinergic agents, and amantadine hydrochloride. Twenty-four control subjects (8 male, 16 female; mean age 61.8±9 years) were healthy volunteers without a major neurologic or psychiatric disorder (including alcoholism, substance abuse, head trauma with consciousness loss, or cerebral vascular disorder). All subjects were given information about the procedure and had given signed informed consent prior to participating in the study.

Experimental protocol

Each patient was instructed to fast for 12 h before the SPECT imaging, in the hope of inducing an "off" state. Patients and control subjects were injected with 740 MBq (20 mCi) of ^{99m}Tc-HMPAO 30 min prior to scanning. Scanning was performed parallel to the canthomeatal line using a dual-head gamma camera VariCam (GE, USA) with a high-resolution collimator (full-width at half-maximum: 8 mm). A polycarbonate head holder was used to reduce head movement during scanning. The acquisition parameters were 120 projections recorded in step-and-shoot mode over a 360° rotation arch. For each head, 60 projections were acquired. The angular step size was 3° and the frame rate was 25 s per step. Each acquisition was completed in 30 min. The acquisition matrix was 128×128; zoom, 1.5.

The reconstruction of SPECT images was achieved using a filtered back projection algorithm with a Metz filter of power 3, resulting in 80 contiguous 128×128 transaxial image slices with in-plane resolution of 1.77×1.77 mm and a slice thickness of 1.8 mm. Attenuation correction based on Chang's method [18] was performed on each slice, with a uniform attenuation coefficient of 0.11.

Image analysis

All images were first converted to Analyze format from their native image format using MRIcro software (http://www.psychology.nottingham.ac.uk/staff/crl/mricro.html) developed by Chris Rorden. Each individual SPECT image was then re-oriented and spatially normalized to the standard Montreal National Institute (MNI) template included in SPM2 (http://www.fil.ion.ucl.ac.uk/spm/) using a 12-parameter affine transformation. Nonlinear SPM algorithms (7×8×7, 12 nonlinear iterations with moderate nonlinear regularization) were used to spatially normalize each subject's image to the SPM SPECT template. As a result, each subject's image was resampled into 2×2×2 mm voxels in a cube with axes right–left, anterior–posterior, and superior–inferior, respectively. After spatial normalization, the individual SPECT images from normal controls (1–24) and patients (25–51) were concatenated, forming a SPECT data matrix, X, with 51 rows (the number of subjects) and 79×95×69 columns (the total number of voxels).

Independent component analysis

ICA decomposition was performed within Matlab (The MathWorks, Inc) under FMRLAB developed by Duann et al. (http://sccn.ucsd.edu/fmrlab) [19]. Within FMRLAB, the off-brain voxels were first removed using an image intensity threshold selected interactively through a graphic user interface. Then, the Bell-Sejnowski information-maximization (Infomax) algorithm [12], as implemented by Makeig et al. [20], was used to derive maximally spatially independent components of the 51 collected images. Applied to our SPECT data matrix, X, ICA found an 'unmixing' matrix, W, that decomposed or linearly unmixed the concatenated SPECT data into a sum of spatially independent components, $U=W×X$, where U is a matrix of spatially fixed independent component SPECT images. Each subject's weight in the column of inverted W matrix represents the relative adjusted rCBF effects in each subject image of the component on the brain regions. After ICA training converged, a logistic regression was applied to the subject weights for each column, using a probability threshold of $p<0.05$, to find "disease-related" components exhibiting a significant weight difference between patients (columns 25–51) and controls (columns 1–24). The remaining components were considered "disease-unrelated" components. Components in these two subspaces were separately back-projected and summed to reconstruct the disease-related and -unrelated portions or subspaces of the individual subject images.

Statistical analysis

SPM analysis was performed on both the reconstructed disease-related and disease-unrelated portions preprocessed by the ICA method described above. In each portion, a 3-D Gaussian filter (16 mm width) was used to smooth each image. The mean CBF of each image was scaled to 50 for each subject.

In both portions, between-group comparisons (controls and PD) were performed on a voxel-by-voxel basis using a general linear model based on the theory of Gaussian fields [21, 22] within SPM. The first comparison sought areas of increased perfusion, and the second, areas of decreased perfusion in PD. The resulting set of voxel values for each comparison constituted a statistical parametric map or SPM $\{t\}$. The SPM$\{t\}$ values were thresholded at the $p<0.001$ uncorrected ($t=3.27$) level; the number and size of connected clusters of suprathreshold voxels were recorded. Corrected (for multiple non-independent comparisons) cluster-level p values were calculated for each cluster based on their spatial extent [20]. Clusters with a corrected p value less than 0.01, which yield >100 voxels, were considered significant. SPM results were then overlaid on a normalized MR image.

Finally, we tested for brain areas in which the ICA-adjusted rCBF changes were correlated with the motor UPDRS score using the SPM (single-subject, covariant-only) method. Data from back projection of the disease-related components set constituted 27 PD subject images. The motor UPDRS score was used as a covariant to look for score-related regions. In this study, voxel clusters above a significance threshold set at the $p<0.003$ uncorrected ($t=3.00$) level and an extent threshold set at a corrected p value less than 0.01 were considered significant.

Results

Table 1 shows the demographic and clinical distribution of the subjects. There was no significant difference in age between controls and patients. In the ICA preprocessed data, nine components were classified by logistic regression as disease-related and 42 components as disease-unrelated.

Significant effects of PD-related changes were extensive in the ICA preprocessed data. In the disease-related component set, PD patients showed increased adjusted rCBF (hyperperfusion) in the bilateral putamen and globus

Table 1 Demography and UPDRS scores of PD and controls

	Controls	PD patients			P value*
		H&Y stage I	H&Y stage II	H&Y stage III	
No.	24	6	10	11	
Age[a]	61.8±9	62.3±11	63.1±13	69.6±6	NS[b]
Sex (M/F)	8/16	2/4	8/2	11/0	<0.05
Motor UPDRS		21.8±4	24.5±9	29.4±8	NS[c]

*P value: compares controls with all PD patients
[a] Mean±SD
[b] NS not significant
[c] Post hoc analysis between H&Y stages I-III was not significant

pallidus, ventral lateral nucleus of thalamus, brainstem, cerebellum, precentral gyrus, superior frontal cortex, and middle occipital gyrus, as well as hypoperfusion in the bilateral middle frontal gyrus (dorsolateral prefrontal cortex), parieto-occipital cortex, superior temporal cortex, insula, and anterior cingulate gyrus. Details of the involved brain areas on the ICA preprocessed data are given in Tables 2 and 3 and in Fig. 1. By contrast, in the disease-unrelated component subspace, not a single brain area showed significant disease-related changes in adjusted rCBF.

In patients, analysis of the disease-related ICA subspace data showed that ICA-adjusted rCBF in the bilateral anterior cingulate, cingulate gyrus, postcentral gyrus, parahippocampus gyrus, right insula, and right inferior parietal lobule were negatively correlated with motor UPDRS scores (Fig. 2). No region showed a positive correlation with motor UPDRS scores. Details of these results are shown in Table 4.

Table 2 Basal ganglion, thalamic nucleus, cerebellum, and brain stem areas showing a significant adjusted CBF difference between PD and controls in disease-related component subspace

Structure	Voxel size[a]	Peak Z value	MNI coordinates (mm)			State
			X	Y	Z	
Basal ganglion						
Caudate head (L)	35	4.77	−6	4	6	−
Caudate head (R)	75	5.22	4	4	6	−
Putamen (L)	559	6.99	−26	−14	2	+
Putamen (R)	145	5.16	28	−18	12	+
Lateral globus pallidus (L)	169	7.77	−24	−16	−2	+
Lateral globus pallidus (R)	55	4.59	24	−16	4	+
Medial globus pallidus (L)	41	6.42	−20	−10	−2	+
Thalamic nucleus						
Medial dorsal nucleus (R)	58	3.98	6	−22	12	−
Ventral lateral nucleus (L)	62	6.29	−18	−16	10	+
Ventral posterior lateral nucleus (L)	45	7.37	−20	−22	2	+
Cerebellum						
Culmen (L)	1,035	6.48	−26	−50	−18	+
Culmen (R)	1,111	6.63	10	−54	−12	+
Declive (L)	764	6.27	−24	−54	−16	+
Declive (R)	487	6.17	10	−56	−16	+
Dentate (L)	203	5.48	−10	−46	−34	+
Dentate (R)	201	4.66	14	−48	−26	+
Fastigium (L)	53	4.64	−8	−48	−28	+
Fastigium (R)	42	4.42	6	−48	−26	+
Anterior lobe (L)	1,707	6.57	−4	−40	−36	+
Anterior lobe (R)	1,744	6.62	10	−54	−12	+
Brain stem						
Midbrain (L)	292	6.28	−2	−32	−14	+
Midbrain (R)	243	6.08	2	−32	−14	+
Pons (L)	618	7.22	−8	−34	−34	+
Pons (R)	536	6.48	4	−28	−32	+
Medulla (L)	131	6.30	−6	−36	−44	+
Medulla (R)	105	5.84	2	−38	−44	+

L left side; R right side; +, adjusted CBF in PD higher than in controls; −, adjusted CBF in PD lower than in controls
[a] Voxel size: 8 mm³

Table 3 Brain areas showing significant adjusted CBF difference between PD and controls in disease-related component subspace

Structure	BA	Voxel size[a]	Peak Z value	MNI coordinates (mm)			State
				X	Y	Z	
Limbic lobe							
Insula (L)	13	559	7.45	−36	−30	18	−
Insula (R)	13	352	4.66	58	−32	20	−
Anterior cingulate (L)	32	297	5.53	−8	38	28	−
Anterior cingulate (R)	32	405	5.70	6	38	28	−
Cingulate gyrus (L)	24	1,435	6.29	−2	−30	44	−
Cingulate gyrus (R)	24	1551	6.30	2	−10	46	−
Posterior cingulate (L)	30	743	7.90	−10	−66	14	−
Posterior cingulate (R)	30	548	7.49	12	−70	14	−
Frontal lobe							
Superior frontal gyrus (L)	9	77	4.79	−20	56	36	+
Superior frontal gyrus (R)	9	170	5.39	16	60	36	+
Medial frontal gyrus (L)	8	151	6.36	−4	44	44	−
Medial frontal gyrus (R)	8	124	5.64	2	42	44	−
Medial frontal gyrus (L)[a]	24	284	5.99	−4	−10	48	−
Medial frontal gyrus (L)	10	230	6.84	−8	64	18	−
Medial frontal gyrus (R)	10	168	7.17	4	68	12	−
Middle frontal gyrus (L)	10	181	5.02	−36	38	14	−
Middle frontal gyrus (R)	8	193	5.96	36	20	50	−
Inferior frontal gyrus (L)	46	207	6.48	−58	36	8	−
Inferior frontal gyrus (R)	47	351	5.53	52	38	−10	+
Orbital gyrus (R)	47	120	5.11	16	26	−28	+
Precentral gyrus (L)	6	362	5.81	−26	−18	58	+
Precentral gyrus (R)	4	201	6.40	34	−24	66	+
Parietal lobe							
Postcentral gyrus (L)	1	48	5.73	−56	−28	44	−
Postcentral gyrus (L)	2	113	7.20	−58	−30	46	−
Postcentral gyrus (L)	3	51	5.71	−58	−26	44	−
Postcentral gyrus (R)	1	43	7.34	66	−22	36	−
Postcentral gyrus (R)	2	94	7.02	66	−22	32	−
Postcentral gyrus (R)	3	88	7.51	62	−18	32	−
Inferior parietal lobule (L)	40	575	7.14	−62	−40	44	−
Inferior parietal lobule (R)	40	540	6.91	68	−26	24	−
Superior parietal lobule (L)	7	275	6.28	−38	−60	58	−
Precuneus (L)	31	551	7.96	−8	−68	16	−
Precuneus (R)	31	539	7.79	10	−72	16	−
Angular gyrus (L)	39	290	7.49	−50	−66	30	−
Occipital lobe							
Middle occipital gyrus (L)	19	124	4.69	−48	−84	12	+
Middle occipital gyrus (R)	19	432	6.00	54	−70	6	+
Cuneus (L)	18	358	7.47	−2	−74	16	−
Cuneus (R)	18	394	7.71	12	−72	16	−
Temporal lobe							
Superior temporal gyrus (L)	38	419	6.29	−50	20	−28	−
Superior temporal gyrus (R)	22	133	5.02	38	−56	20	−
Middle temporal gyrus (L)	19	97	4.46	−52	−82	14	+
Middle temporal gyrus (R)	39	975	6.54	54	−682	10	+
Inferior temporal gyrus (L)	20	242	6.29	−34	−2	−50	+
Inferior temporal gyrus (R)	20	289	4.42	50	−16	−36	+
Fusiform gyrus (L)	37	41	4.42	−56	−50	−22	+
Fusiform gyrus (R)	37	49	5.31	38	−54	−16	+
Parahippocampal gyrus (L)	36	85	4.96	−32	−30	−26	−

L left side; *R* right side; *BA* Brodmann area; +, adjusted CBF in PD higher than in controls; −, adjusted CBF in PD lower than in controls
[a] Voxel size: 8 mm^3

Fig. 1 Maximum intensity projection on 3-D rendered brain showing SPM group difference results after ICA preprocessing. Highlighted brain areas show significant ICA-adjusted rCBF changes in PD compared with normal controls. Results are plotted on a 3-D rendered brain template from SPM2. A warm color represents hyperperfusion and a cold color, hypoperfusion of ICA-adjusted rCBF in PD. *T* value represents the severity of rCBF changes
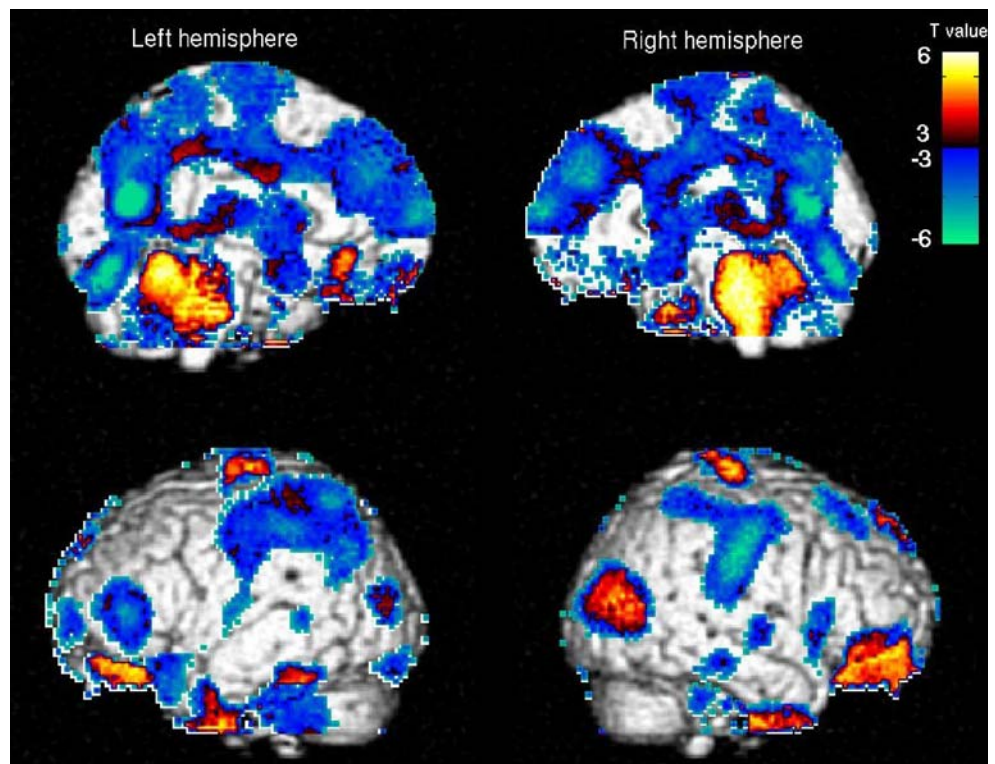
Discussion

By first applying spatial ICA to eliminate disease-unrelated signal change variability, and then using SPM to assess the statistical significance, we were able to observe adjusted rCBF changes between groups. In the disease-related data subspace, many brain areas showed significant ICA-adjusted rCBF group differences, including hypoperfusion in the supplementary motor area and hyperperfusion in various basal ganglion nuclei. By contrast, in the complementary disease-unrelated subspace, no significant group differences existed. The findings are consistent with predictions from the basal ganglia circuit model of PD [2, 3]. These results demonstrate that image preprocessing using ICA can further separate disease-related from disease-

unrelated signal changes in SPECT images and improve study results.

ICA-adjusted rCBF increases in PD

We found that in PD, the adjusted rCBF is increased in the basal ganglia, thalamus, brainstem, and cerebellum. Among these regions, an increased adjusted rCBF in the bilateral putamen, globus pallidum, thalamus, and pons is to be expected according to the basal ganglia circuit model [2, 3]. This is also consistent with findings from previous studies using SPECT and FDG-PET [9, 23]. Our findings of increased ICA-adjusted CBF in the globus pallidum and thalamus are also in agreement with the fact that surgical ablation or deep brain stimulation of these regions improves

Fig. 2 Correlations between motor UPDRS scores and adjusted rCBF. Adjusted rCBF in the left anterior cingulate gyrus was negatively correlated with motor UPDRS scores ($r = 0.75$)
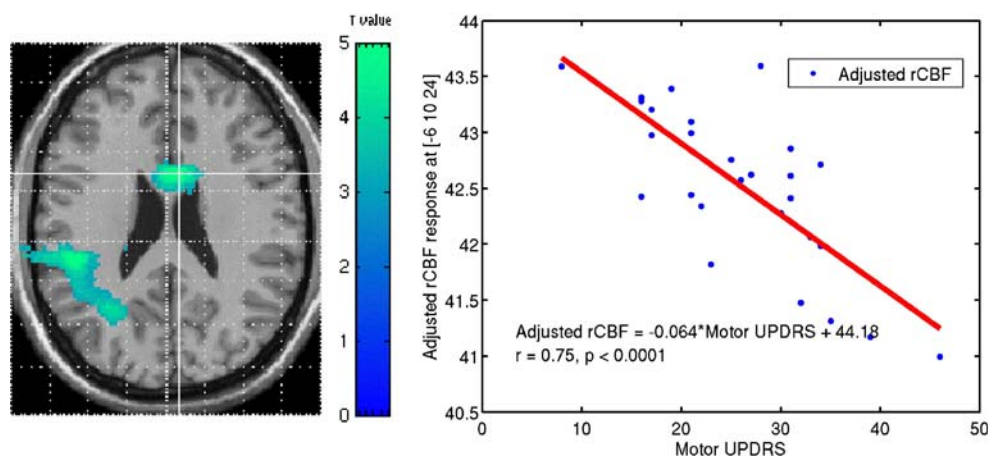
Table 4 Brain areas showing a significant correlation with motor UPDRS scores

Structure	BA	Voxel size[a]	Peak Z value	MNI coordinates (mm)		
Negative correlations				X	Y	Z
Cingulate gyrus (L)	24	72	4.19	−2	8	30
Cingulate gyrus (R)	31	89	4.69	14	−32	44
Anterior cingulate (L)	33	44	5.74	−6	10	24
Anterior cingulate (R)	24	36	4.70	4	14	28
Insula (R)	13	97	5.11	42	−32	18
Precentral gyrus (L)	4	101	4.10	−56	−14	32
Inferior parietal lobule (R)	40	242	6.00	46	−34	34
Postcentral gyrus (L)	43	78	3.71	−56	−16	34
Postcentral gyrus (R)	2	215	5.91	48	−32	38
Superior temporal gyrus (R)	29	457	5.57	40	−32	16
Fusiform gyrus (R)	20	92	5.15	54	−20	−28
Parahippocampal gyrus (L)	36	145	6.14	−26	−16	−32
Uncus (L)	28	51	4.40	−16	2	−30
Pons (L)		45	4.45	−10	−12	−32

L left side, *R* right side, *BA* Brodmann area
[a] Voxel size: 8 mm^3

clinical symptoms in PD [24, 25]. This may imply that neuronal hyperactivity in these regions, reflected as hypermetabolism in this study, is responsible for parkinsonian symptoms. Increased ICA-adjusted rCBF in the putamen may result from more complex feedback mechanisms primarily induced by striatal dopamine deficiency [26]. Results from previous SPECT and FDG-PET studies regarding cerebellar blood flow have been contradictory. The increased cerebellar rCBF found in our study agrees with some previous reports [9], including that of Hilker et al. [27], who found a relatively increased left rostral cerebellar rCMR in advanced PD patients prior to surgery. In another FDG and fluoro-L-dopa PET study, Ghaemi et al. [28] also found cerebellar metabolic hyperactivity in PD, which is more closely related to akinesia and rigidity than to tremor. However, our results did not show any correlation between motor UPDRS scores and cerebellar hyperperfusion. We did not further divide the motor UPDRS scores into akinesia, rigidity, and tremor subcategories to correlate each symptom with metabolic changes. We think the motor UPDRS scores, which are by nature only semiquantitative, may not be a reliable clinical indicator if further divided.

Our patients also showed a relative hyperperfusion in the middle and inferior temporal and fusiform gyri. This may be related to the antiparkinsonian treatment these patients were receiving, since medication and deep brain stimulation can both activate regions, including the temporal gyri [29]. Nonpsychotic visual hallucinations in PD may also be associated with hyperperfusion in the right temporal gyrus

and hypoperfusion in the fusiform gyrus, as reported by Oishi et al. [30].

ICA-adjusted rCBF decreases in PD

There was a widely distributed decrease in ICA-adjusted rCBF in the cerebral cortex of parkinsonian patients. Involved regions included posterior parieto-occipital cortex, precuneus, cingulate, insula, inferior frontal, dorsolateral prefrontal cortex, and supplementary motor cortex. In addition, the caudate and medial dorsal nucleus of the thalamus also showed decreases in ICA-adjusted rCBF.

Firbank et al. [31] and Antonini et al. [32], using SPECT to study PD patients with cognitive impairment, both found that demented PD patients had significant perfusion decrements in all the cortical areas, particularly in temporal and parietal regions. Another factor that may be responsible for decreased rCBF in parietotemporal cortex is autonomic failure. Arahata et al. [33] reported that rCMR in the cerebral cortex in PD with autonomic failure was markedly reduced, particularly in occipital cortex, inferior parietal cortex, and superior parietal cortex.

Our patients showed relative hypoperfusion in the inferior frontal cortex. Hypometabolism in the inferior frontal cortex has been reported in advanced PD and in PD with depression by FDG-PET study [34, 35]. The observed abnormalities in these brain regions are probably more related to neuropsychiatric symptoms in PD [36].

We also found hypoperfusion in insula and bilateral cingulate cortex. Various rCBF changes (increases [9] or decreases [23]) in the insula have been reported in PD. Most PET and SPECT studies have not reported decreased rCMR or rCBF in the cingulate gyrus. In a SPECT study on PD patients treated with deep brain stimulation to the subthalamic nucleus, Sestini et al. [37] demonstrated a significant stimulation-induced increase in rCBF in the right presupplementary motor area, anterior cingulate cortex, dorsolateral prefrontal cortex, and medial Brodmann's area 8. Their results provide direct evidence of the association between the basal ganglia circuit and the limbic system, and imply that hypoperfusion in these areas may account for an impairment of the higher-order aspects of motor control. Thus insular and cingulate hypoperfusion in PD in the present study is more consistent with the extended predictions of the basal ganglia circuit model.

ICA-adjusted rCBF correlates with the motor UPDRS scores

We found a negative correlation between the motor UPDRS scores and the ICA-adjusted rCBF in the bilateral cingulate, anterior cingulate, postcentral gyrus, right inferior parietal lobule, insula, and fusiform gyrus. Previous studies corre-

lating PD neural substrate with ratings of clinical symptoms had produced inconsistent results [23, 38, 39], possibly because they were carried out using different imaging techniques (e.g. PET vs SPECT) and different clinical evaluating tools. Hypoperfusion in the cingulate gyrus had been shown to relate to PD with predominant postural instability and gait difficulty [40]. Studies utilizing either univariate or multivariate methods did find a correlation of UPDRS score with insular activities, but not with cingulate activities [10, 23]. Our results not only demonstrated hypoperfusion in the anterior cingulate, cingulate gyrus, and insular regions, but also a negative correlation of perfusion in these regions with motor UPDRS scores. This may suggest that both insular and cingulate hypoperfusion have a relation with disease severity and participate in motor performance. Our findings of a negative correlation between motor UPDRS and the rCMR in the inferior parietal cortex and visual association cortex are supported by the findings of others [23, 39]. These results demonstrate that the abnormally decreased perfusion in specific cortical regions is quantitatively related to the severity of Parkinson's disease.

Conclusion

In the present study, we assessed adjusted rCBF differences between PD patients and normal controls using independent component analysis (ICA) as a data processing tool. The ICA-adjusted rCBF changes in various brain areas found by this method were compatible with the standard pathophysiological model of PD. Our data also showed hypoperfusion in the insula and cingulate gyrus in PD that was negatively correlated with motor UPDRS scores. We think that ICA preprocessing is a useful complement for purely hypothesis-driven methods of analyzing group SPECT data differences. This method might be useful in developing alternative and/or more comprehensive disease and brain circuit models for PD or other neurodegenerative diseases.

References

1. Hornykiewcz O. Dopamine (3-hydroxytyramine) and brain function. Pharmacol Rev 1966;18:925–64.
2. Albin RL, Young AB, Penney JB. The functional anatomy of basal ganglia disorders. Trends Neurosci 1989;12:366–75.
3. Alexander GE, Crutcher MD. Functional architecture of basal ganglia circuits: neural substrates of parallel processing. Trends Neurosci 1990;13:266–71.
4. Holman BL, Johnson KA, Gerada B, Carvalho PA, Satlin A. The scintigraphic appearance of Alzheimer's disease: a prospective study using technetium-99m-HMPAO SPECT. J Nucl Med 1992;32:181–5.
5. Perlmutter JS, Raichle ME. Regional blood flow in hemiparkinsonism. Neurology 1985;35:1127–34.
6. Henriksen L, Boas J. Regional cerebral blood flow in hemiparkinsonian patients: emission computerized tompgraphy of inhaled 133Xenon before and after levodopa. Acta Neurol Scand 1985;71:257–66.
7. Wolfson LI, Leenders KL, Brown LL, Jones T. Alterations of cerebral blood flow and oxygen metabolism in Parkinson's disease. Neurology 1985;35:1399–405.
8. Pizzolato G, Dam M, Borsato N, Saitta B, Da Col C, Perlotto N, et al. ^{99m}Tc-HMPAO SPECT in Parkinson's disease. J Cereb Blood Flow Metab 1988;8(suppl):S101–8.
9. Imon Y, Matsuda H, Ogawa M, Kogure D, Sunohara N. SPECT image analysis using statistical parametric mapping in patients with Parkinson's disease. J Nucl Med 1999;40;1583–9.
10. Vaasinen V, Maguire RP, Hundemer HP, Leenders KL. Corticostriatal covariance patterns of 6-[F18]fluoro-L-dopa and [F18]fluorodeoxy-glucose PET in Parkinson's disease. J Neurol 2006;253:340–8.
11. Dujardin K, Defebvre L, Duhamel A, Lecouffe P, Rogelet P, Steinling M, et al. Cognitive and SPECT characteristics predict progression of Parkinson's disease in newly diagnosed patients. J Neurol 2004;251:1383–92.
12. Bell AJ, Sejnowski TJ. An information-maximization approach to blind separation and blind deconvolution. Neural Comput 1995;7(6):1129–59.
13. Jung T-P, Makeig S, McKeown MJ, Bell AJ, Lee T-W, Sejnowski TJ. Imaging brain dynamics using independent component analysis. Proc IEEE 2001;89:1107–22.
14. McKeown MJ, Makeig S, Brown GG, Jung T-P, Kindermann SS, Sejnowski TJ. Analysis of fMRI by blind separation into independent spatial components. Hum Brain Mapp 1988:6:160–88.
15. Ward CD, Gibb WR. Research diagnostic criteria for Parkinson's disease. Adv Neurol 1990;53:245–9.
16. Hoehn MM, Yahr MD. Parkinsonism: onset, progression and mortality. Neurology 1967;17:427–42.
17. Fahn S, Elton RL, Members of the UPDRS Development Committee. Unified Parkinson's disease and movement disorders. In: Fahn S, Marsden CD, Calne DB, Goldstein M, editors. Recent developments in Parkinson's disease vol 2. Florham Park: NJ Mcmillan Health Care Information; 1987. pp. 153–64.
18. Chang LT. A method for attenuation correction in radionuclide computed tomography. IEEE Trans Nucl Sci 1978;25:638–43.
19. Duann JR, Jung TP, Kuo WJ, Yeh TC, Makeig S, Hsieh JC, et al. Single-trial variability in event-related BOLD signals. Neuroimage 2002;15:823–35.
20. Makeig S, Jung TP, Bell AJ, Ghahremani D, Sejnowski TJ. Blind separation of auditory event-related brain responses into independent components. Proc Natl Acad Sci USA 1997;94:10979–84.
21. Friston KJ, Frith CD, Liddle PF, Frackowiak RSJ. Comparing functional (PET) images: the assessment of significant change. J Cereb Blood Flow Metab 1991;11:690–9.
22. Friston KJ, Worsley KJ, Frackowiak RSJ, Mazziotta JC, Evans AC. Assessing the significance of focal activations using their spatial extent. Hum Brain Mapp 1994;1:214–20.
23. Kikuchi A, Takeda A, Kimpara T, Nakagawa M, Kawashima R, Sugiura M, et al. Hypoperfusion in the supplementary motor area, dorsolateral prefrontal cortex and insular cortex in Parkinson's disease. J Neurol Sci 2001;193:29–36.
24. Dogali M, Fazzini E, Kolodny E, Eidelberg D, Sterio D, Devinsky O, et al. Stereotactic ventral pallidotomy for Parkinson's disease. Neurology 1995;45:753–61.
25. Alvarez L, Macias R, Lopez G, Alvarez E, Pavon N, Rodriguez-Oroz MC, et al. Bilateral subthalamotomy in Parkinson's disease: initial and long-term response. Brain 2005;128:570–83.

26. Antonini A, Vontobel P, Psylla M, Gunther I, Maguire PR, Missimer J, et al. Complememtary positron emsission tomographic studies of the striatal dopaminergic system in Parkinson's disease. Arch Neurol 1995;52:1183–90.

27. Hilker R, Voges J, Weisenbach S, Kalbe E, Burghaus L, Ghaemi M, et al. Subthalamic nucleus stimulation restores glucose metabolism in associative and limbic cortices and in cerebellum: evidence from a FDG-PET study in advanced Parkinson's disease. J Cereb Blood Flow Metab 2004;24:7–16.

28. Ghaemi M, Raethjen J, Hilker R, Rudolf J, Sobesky J, Deuschl G, et al. Monosymptomatic resting tremor and Parkinson's disease: a multitracer positron emission tomographic study. Mov Disord 2002;17:782–8.

29. Goerendt IK, Lawrence AD, Mehta MA, Stern JS, Odin P, Brooks DJ. Distributed neural actions of anti-parkinsonian therapies as revealed by PET. J Neural Transm 2006;113:75–86.

30. Oishi N, Udaka F, Kameyama M, Sawamoto N, Hashikawa K, Fukuyama H. Regional cerebral flow in Parkinson disease with nonpsychotic visual hallucinations. Neurology 2005;65:1708–15.

31. Firbank MJ, Colloby SJ, Burn DJ, McKeith IG, O'Brien JT. Regional cerebral blood flow in Parkinson's disease with and without dementia. Neuroimage 2003;20:1309–19.

32. Antonini A, De Notaris R, Benti R, De Gaspari D, Pezzoli G. Perfusion ECD/SPECT in the characterization of cognitive deficits in Parkinson's disease. Neurol Sci 2001;22:47–8.

33. Arahata Y, Hirayama M, Ieda T, Koike Y, Kato T, Tadokoro M, et al. Parieto-occipital glucose hypometabolism in Parkinson's disease with autonomic failure. J Neurol Sci 1999;163:119–26.

34. Mayberg HS, Starkstein SE, Sadzot B, Preziosi T, Andrezejewski PL, Dannals RF, et al. Selective hypometabolism in the inferior frontal lobe in depressed patients with Parkinson's disease. Ann Neurol 1990;28:57–64.

35. Berding G, Odin P, Brooks DJ, Nikkhah G, Matthies C, Peschel T, et al. Resting regional cerebral glucose metabolism in advanced Parkinson's disease studied in the off and on conditions with [^{18}F] FDG-PET. Mov Disord 2001;16:1014–22.

36. Black KJ, Hershey T, Hartlein JM, Carl JL, Perlmutter JS. Levodopa challenge neuroimaging of levodopa-related mood fluctuations in Parkinson's disease. Neuropsychopharmacology 2005;30:590–601.

37. Sestini S, Scotto di Luzio A, Ammannati F, De Cristofaro MT, Passeri A, Martini S, et al. Changes in regional cerebral blood flow caused by deep-brain stimulation of the subthalamic nucleus in Parkinson's disease. J Nucl Med 2002;43:725–32.

38. Lozza C, Marie RM, Baron JC. The metabolic substrates of bradykinesia and tremor in uncomplicated Parkinson's disease. Neuroimage 2002;17:688–99.

39. Nagano-Saito A, Kato T, Arahata Y, Washimi Y, Nakamura A, Abe Y, et al. Cognitive- and motor-related regions in Parkinson's disease: FDOPA and FDG PET studies. Neuroimage 2004;22:553–61.

40. Mito Y, Yoshida K, Yabe I, Makino K, Tashiro K, Kikuchi S, et al. Brain SPECT analysis by 3D-SSP and phenotype of Parkinson's disease. J Neurol Sci 2006;241:67–72.